J Membrane Biol (2010) 238:69–80
DOI 10.1007/s00232-010-9320-z

Electroporation-Induced Inward Current in Voltage-Clamped Guinea Pig Ventricular Myocytes

Oksana Dyachok · Pavel Zhabyeyev · Terence F. McDonald

Received: 13 September 2010 / Accepted: 29 October 2010 / Published online: 21 November 2010

Abstract Electroporation induced by high-strength electrical fields has long been used to investigate membrane properties and facilitate transmembrane delivery of molecules and genes for research and clinical purposes. In the heart, electric field-induced passage of ions through electropores is a factor in defibrillation and postshock dysfunction. Voltage-clamp pulses can also induce electroporation, as exemplified by findings in earlier studies on rabbit ventricular myocytes: Long hyperpolarizations to ≤ -110 mV induced influx of marker ethidium and irregular inward currents that were as large with external $NMDG^+$ as Na^+. In the present study, guinea pig ventricular myocytes were bathed with $NMDG^+$, Na^+ or $NMDG^+ + La^{3+}$ solution (36°C) and treated with five channel blockers. Hyperpolarization of myocytes in $NMDG^+$ solution elicited an irregular inward current (I_{ep}) that reversed at -21.5 ± 1.5 mV. In myocytes hyperpolarized with 200-ms steps every 30 s, I_{ep} occurred in "episodes" that lasted for one to four steps. Boltzmann fits to data on the incidence of I_{ep} per experiment indicate 50% incidence at -129.7 ± 1.4 mV (Na^+) and -146.3 ± 1.6 mV ($NMDG^+$) (slopes ≈ -7.5 mV). I_{ep} amplitude increased with negative voltage and was larger with Na^+ than $NMDG^+$ (e.g., -2.83 ± 0.34 vs. -1.40 ± 0.22 nA at -190 mV). La^{3+} (0.2 mM) shortened episodes, shifted 50% incidence by -35 mV and decreased amplitude, suggesting that it inhibits opening/promotes closing of electropores. We compare our findings with earlier ones, especially in regard to electropore selectivity. In the Appendix, relative permeabilities and modified excluded-area theory are used to derive estimates of electropore diameters consistent with reversal potential -21.5 mV.

Keywords Cardiomyocyte · Electroporation-induced current · $NMDG^+$ · Lanthanum · Electropore ion selectivity

Introduction

The effects of strong electrical fields on the electrical properties and permeability of membranes have been studied for more than five decades in preparations ranging from the nerve axon (Hodgkin 1947) and node of Ranvier (Del Castillo and Katz 1954; Stämpfli 1958) to red blood cells (Zimmermann et al. 1976), heart cells (Jones et al. 1978), microorganisms (Sale and Hamilton, 1967) and bilayer lipid membranes (Huang et al. 1964; Tien and Diana 1967). In his article, Stämpfli (1958) referred to the current-injected node of Ranvier undergoing reversible and irreversible membrane electrical breakdown and proposed that breakdown was related to brief disarrangement of bilayer lipids and consequent transmembrane passage of ions. Ooyama and Wright (1961) also studied current-injected node of Ranvier and attributed membrane breakdown at -210 and -275 mV to the opening of "holes" in the membrane. In the interim, notions of holes, "defects" (Abidor et al. 1979) and "microlesions" (Jones et al. 1987) have given way to the view that membrane breakdown (electroporation, electropermeabilization) involves the formation of lipid pores (e.g., Kinosita and Tsong 1977; Tsong 1983; Chernomordik et al. 1987) that are lined by the charged heads of phospholipid groups from the inner leaflet (Vernier et al. 2004; Hu et al. 2006).

O. Dyachok · P. Zhabyeyev · T. F. McDonald (✉)
Department of Physiology and Biophysics, Dalhousie University, Halifax, NS B3H 1X5, Canada
e-mail: terence.mcdonald@dal.ca

The vast majority of studies on the effects of strong electrical fields have focused on experimental and theoretical investigation of electroporation of cells induced by short-duration (nanoseconds to milliseconds), high-strength external electrical fields that rapidly shift cell membrane potential to electroporation-threshold levels of 250–1,000 mV (for recent reviews, see Chen et al. 2006; Escoffre et al. 2007; Wang et al. 2010). This mode of electroporation has applications not only in cell function research (e.g., Schoenbach et al. 2004; Kitamura et al. 2008; Uesaka et al. 2008) but also in industry (Schoenbach et al. 2000) and clinical delivery of drugs and genes to cells (Dev et al. 2000; Heller and Heller 2006; Sersa et al. 2008). In addition to the latter aspect (e.g., Harrison et al. 1998; Kim et al. 2006), electroporation of heart cells caused by defibrillator-type electrical shocks (Jones et al. 1987; Al-Khadra et al. 2000) is an important factor in both defibrillation and postshock cardiac dysfunction (Tung 1992; Fedorov et al. 2008).

There have been relatively few investigations of electroporation of whole cell–configured heart cells induced by electrical fields applied in the form of voltage-clamp commands. Bonvallet and Christé (1988) reported that a 1.36-s hyperpolarization of a frog atrial myocyte to −260 mV induced a novel inward current of ≈−0.5 nA amplitude. The current featured jagged deflections and an irregular time course, and they attributed its development to membrane electrical breakdown of the type postulated by Stämpfli (1958). Ochi and colleagues (Akuzawa-Tateyama et al. 1998; Song and Ochi 2002) applied minutes-long staircase hyperpolarizations and 40-s step hyperpolarizations to guinea pig ventricular myocytes and recorded fluctuating jagged inward currents whose amplitudes ranged from tens of picoamperes at −110/−120 mV to several nanoamperes at −190 mV. Based on findings that the irregular inward currents reversed near 0 mV, were unaffected by replacement of external Na^+ by large (196 Da) $NMDG^+$, were inhibited by 0.1–0.5 mM La^{3+} and coincided with uptake of ethidium bromide (ethidium$^+$, 314 Da) dye, they attributed the currents to passage of ions through electropores.

The present study arose from investigation of the effects of voltage-dependent blockers Cs^+ and Ba^{2+} on inwardly rectifying K^+ current (I_{K1}) at negative potentials in guinea pig ventricular myocytes. We found that relatively short (200–1,000 ms) hyperpolarizations elicited irregular jagged inward currents in myocytes superfused with $NMDG^+$ solution. Based on elimination of other candidates and resemblance of current records to records presented in earlier publications (see above), we deemed that the currents were due to electroporation and went on to characterize them in terms of reversal potential, incidence, amplitude, effects of replacement of external Na^+ by $NMDG^+$ and inhibition by La^{3+}.

Methods

Preparation of Myocytes

Experimental protocols for animal studies were approved by the Animal Care Committee of Dalhousie University in accord with the guidelines established by the Canadian Council on Animal Care. Adult guinea pigs (250–300 g) were killed by cervical dislocation, and the hearts were quickly removed, mounted on a Langendorff column and perfused through the coronary artery for 10–15 min. The Ca^{2+}-free perfusate (37°C) contained (in mM) NaCl 125, KCl 5, $MgCl_2$ 1.2, taurine 20, glucose 20 and *N*-2-hydroxyethylpiperazine-*N'*-2-ethanesulfonic acid (HEPES) 5 (pH 7.4), as well as 0.08–0.12 mg/ml collagenase (Yakult Pharmaceutical, Tokyo, Japan). On completion of collagenase digestion, the heart tissue was minced and myocytes dispersed in a high-K^+, nutrient-supplemented storage solution (22°C) that contained KCl 30, KOH 80, KH_2PO_4 30, $MgSO_4$ 3, glutamic acid 50, taurine 20, glucose 20, ethylene glycol-bis(*β*-aminoethyl ether)-*N*,*N*,*N*′,*N*′-tetra-acetic acid (EGTA) 0.5 and HEPES 10 (pH 7.4 with KOH).

Electrophysiology

A few drops of myocyte suspension were placed in a 0.3-ml chamber mounted on the stage of an inverted phase-contrast microscope, and the chamber was perfused with bathing solution (see below) at a flow rate near 3 ml/min. Rod-shaped quiescent myocytes were voltage-clamped using the standard ruptured-patch method. Recording pipettes were fabricated from thick-walled borosilicate glass capillaries (H15/10/137; Jencons Scientific, Leighton Buzzard, UK) and had resistances of 2–3 MΩ when filled with pipette solution. Pipette offsets were nulled prior to patch formation, and liquid junction potentials (≈−10 mV) were offset during data analysis. Membrane currents were recorded with an EPC-9 amplifier (Heka Electronics, Mahone Bay, Canada), filtered at 3 kHz and digitized with Pulse software (Heka Electronics) at a sampling rate of 12 kHz. Data files were converted from Pulse to Axon format and analyzed with Clampfit electrophysiology software (Axon Instruments, Union City, CA). All experiments were conducted at 36°C.

Bathing and Pipette Solutions

The Na^+ solution used to bathe myocytes contained (in mM) NaCl 140, KCl 5.4, $CaCl_2$ 1.8, $MgCl_2$ 1, glucose 10 and HEPES 5 (pH 7.4), as well as 1 mM Cd^{2+}, 3 μM E4031 and 3–5 μM glibenclamide. $NMDG^+$ bathing solution was made by equimolar substitution of Na^+ by $NMDG^+$. The pipette solution contained (in mM) KCl 30,

potassium aspartate 110, MgATP 5, EGTA 5 and HEPES 5 (pH 7.2).

Chemicals and Drugs

All chemicals used in making solutions were purchased from Sigma-Aldrich (Oakville, Canada) and were of the highest purity grade available. E4031 was purchased from Tocris Bioscience (Ellisville, MO), and glibenclamide was from Sigma-Aldrich.

Statistics

Experimental data are expressed as means ± SEM; *n* represents the number of experiments. Tests used for statistical comparisons are given in the results. Differences were considered significant at $P < 0.05$.

Results

In the experiments described below, myocytes were held at a potential near the calculated E_K (−86 mV) and bathed in a modified Tyrode's solution that contained 1 mM Cd^{2+}, 3 μM E4031 and 3–5 μM glibenclamide. The principal external cation was either Na^+ (Na^+ solution) or $NMDG^+$ (Na^+-free $NMDG^+$ solution).

Irregular Inward Current Induced by Voltage-Ramp Sequences

As noted above, we first observed an irregular inward current component while investigating block of inwardly rectifying I_{K1} by Cs^+. Since block by Cs^+ is voltage- and concentration-dependent (Harvey and Ten Eick 1989), we used voltage ramps as a convenient means of sweeping the voltage range of interest. Figure 1 shows records of currents elicited by voltage ramp sequences (200-ms step from holding potential −85 to −190 mV, 1.9-s ramp to 0 mV, 200-ms hold at 0 mV). The sequences were applied to the myocyte every 30 s just before and during treatment with 1 mM Cs^+ and during subsequent cotreatment with the more potent I_{K1} blocker Ba^{2+} (1 mM). Although the currents in Fig. 1a had the expected waveforms, that was not the case for the currents recorded 2 min before and 2 min after the Fig. 1a Cs^+ trace. In the earlier of these, there was superimposition of a fluctuating inward-directed current that began ≈150 ms into the −190-mV step and subsided as the ramp reached −170 mV (Fig. 1b); in the later one, the irregular inward component developed earlier and did not subside as quickly (Fig. 1c). Surprisingly, the currents recorded immediately before and after the latter current lacked extra inward components (Fig. 1c). The same was

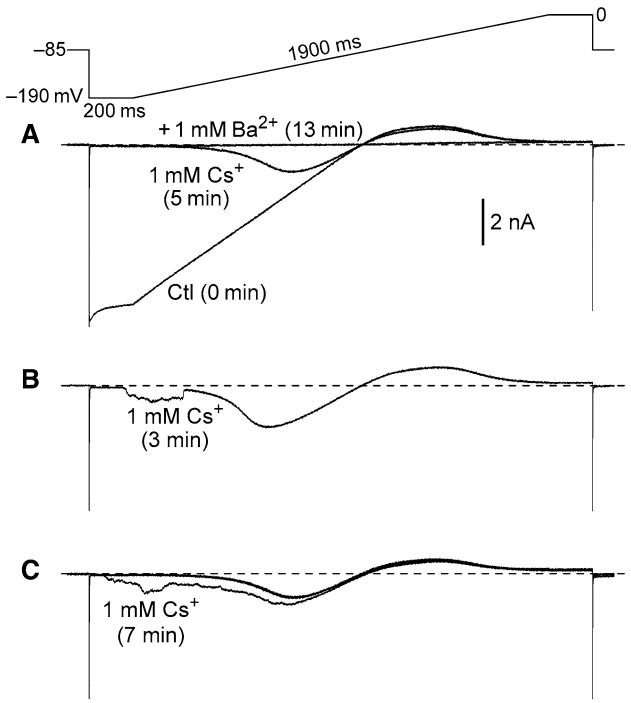

Fig. 1 Current records elicited by voltage ramp sequences. The myocyte was bathed in $NMDG^+$ solution, and voltage ramp sequences (*top*) were applied every 30 s before and during treatment with Cs^+ and during subsequent cotreatment with Ba^{2+}. Times on the records are continuous; Cs^+ was added at 0 min and Ba^{2+} at 10 min. *Dashed lines* indicate zero-current levels. **a** The control (*Ctl*) record shows inwardly rectifying I_{K1}, the Cs^+ record reflects voltage-dependent block of I_{K1} and the Ba^{2+} record shows near-complete block. **b** Record obtained 2 min before the Cs^+ record in **a**. Note the irregular inward current component at early times. **c** Records obtained on three consecutive steps several minutes after the Cs^+ record in **a**. The second of these records displays irregular inward current

true of the ramp currents recorded just before and after the one in Fig. 1b (not shown).

In some experiments with $NMDG^+$ solution that contained 1–20 mM Cs^+ and 1–3 mM Ba^{2+}, ramp sequences triggered long-lasting inward currents. In the example shown in Fig. 2a, the ramp evoked an inward current that declined with voltage in a quasi-linear fashion and crossed the voltage axis at −18 mV. This was taken as the reversal potential (E_{rev}) of the inward current in this myocyte. In 11 experiments in which a ramp sequence induced a persistent inward current, E_{rev} was −21.5 ± 1.5 mV.

Examples of preramp currents and postramp inward tail currents (ramp-sequence current sections removed) are shown in Fig. 2b. Some of the tail currents increased in amplitude over the 500-ms time frame of the tail records (suggesting redevelopment of current), some decreased and others were nearly unchanged. However, these were short-term trends; in nine experiments that featured large tails, the amplitude of the current at the 100-ms postramp sequence was −1.24 ± 0.13 nA and the amplitude 27.5 s

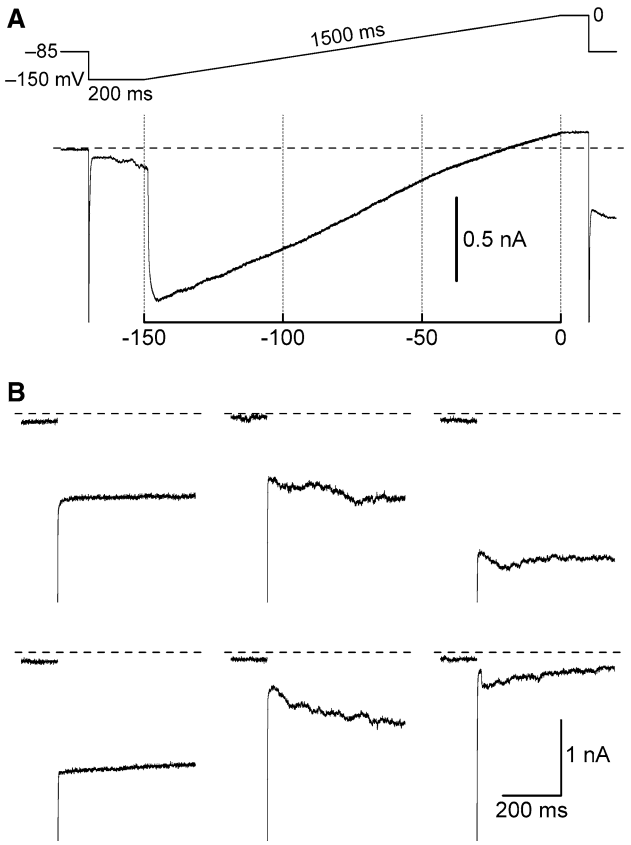

Fig. 2 Quasi-linear *I–V* relation and postramp inward tail currents associated with persistent I_{ep}. Myocytes were held at −85 mV, bathed in $NMDG^+$ solution and treated with 3–20 mM Cs^+ and 1–3 mM Ba^{2+}. *Dashed lines* indicate zero-current levels. **a** Current elicited by a voltage ramp sequence (*top*). The voltage at zero-current (E_{rev}) is −18 mV. **b** Examples of preramp holding currents (*left side of each panel*) and associated postramp inward tail currents (*right side of each panel*) recorded from six myocytes in which voltage ramp sequences triggered persistent I_{ep}. Note the variable configuration of the tail currents

later at the 100-ms preramp sequence was −0.14 ± 0.02 nA. Since the preramp sequence current amplitude prior to development of the inward current was −0.05 ± 0.01 nA, these values indicate an average decay >90% during the interval at −85 mV.

It seemed likely that the irregular inward current under investigation was carried by hyperpolarization-induced electropores rather than by ion channels. The channels that might have been open (or activated) at ≤−150 mV include CLC-2 channels, K_{ATP} channels, hyperpolarization-activated I_f-carrying cation channels and nonselective cation channels. Their contributions to an irregular inward current can be discounted as follows: (1) inwardly rectifying CLC-2 Cl^- current is fully blocked by 1 mM Cd^{2+} (Huang et al. 2009); (2) $I_{K,ATP}$, which can have an irregular time course (Noma and Shibasaki 1985; Clapp 1995), should have been prevented by dialysate ATP and blocked by glibenclamide; (3) Na^+-dependent I_f should have been diminished in $NMDG^+$ solution and completely blocked by 2–4 mM Cs^+ (Hagiwara and Irisawa 1989; Yu et al. 1993); and (4) current carried by nonselective cation channels (whole-cell conductance ≈230 pS in Na^+ solution; Kiyosue et al. 1993) should have been very small in $NMDG^+$ solution (Isenberg 1993; Kiyosue et al. 1993) and, to the extent that it is TRPM7 channel current, strongly blocked by dialysate Mg^{2+}/MgATP and external divalent cations (Gwanyanya et al. 2004). Based on the foregoing considerations, we termed the hyperpolarization-induced inward current "I_{ep}" and investigated it further by using voltage steps rather than ramps.

I_{ep} in Myocytes Regularly Pulsed to Negative Test Potentials

The occurrence and amplitude of I_{ep} in myocytes treated with 5–20 mM Cs^+ ± 1–3 mM Ba^{2+} was investigated by applying 200-ms hyperpolarizing steps every 30 s to a fixed potential and scrutinizing the current records for the presence of I_{ep}.

Episodes of I_{ep}

In line with the results shown in Fig. 1, we found that step-induced I_{ep} waxed and waned at particular times during the experiments. By scoring current traces as having $I_{ep} > 100$ pA or not, we could identify "outbreaks" (episodes) of I_{ep}. Data illustrating the occurrence of such episodes are shown in Fig. 3a (left: I_{ep} off, on, off, on successive steps; right: I_{ep} increasing over several steps [before subsiding in a similar manner; not shown]) as well as in Fig. 3b (I_{ep} off, on, on, off).

Ninety-four episodes were identified in 81 experiments in which myocytes were bathed in Na^+ or $NMDG^+$ solution and regularly pulsed to either −160 or −190 mV. After normalization of end-of-step I_{ep} amplitudes during an episode to the maximum (=1.0) during that episode and moderate "shoehorning" of normalized I_{ep} amplitude, we found that episodes could be classified into five types plus one "other." (The exact number of types is unimportant; the purpose of the classification was to determine broad patterns.) As indicated by the fractions below the episode types in Fig. 3c, I_{ep} amplitude frequently (>82% of episodes) reached a peak value on the first step of an episode. A second finding of interest was that a slight majority of the episodes were of the off–on–off variety, primarily due to their frequency at −160 mV (65 vs. 29% at −190 mV). Data from myocytes bathed with $NMDG^+ + La^{3+}$ (0.2 mM) solution are not included in Fig. 3c. In these myocytes, 65% of 20 episodes at −190 mV were of the off–on–off type.

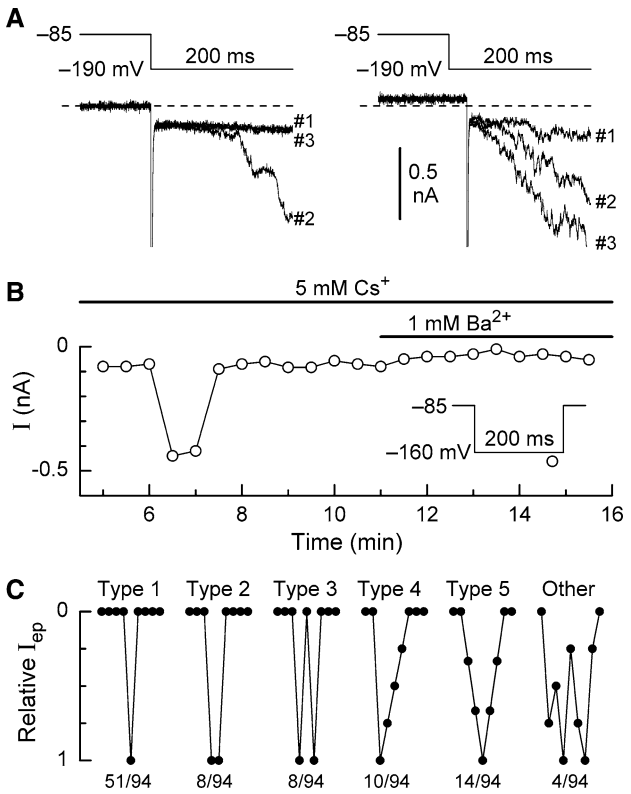

Fig. 3 Episodes of I_{ep} in myocytes regularly pulsed to −190 or −160 mV. Myocytes were bathed in $NMDG^+$ solution (**a**–**c**) or in Na^+ solution (**c**) and treated with 5–20 mM Cs^+ and 1–3 mM Ba^{2+}. They were held at −85 mV and pulsed with 200-ms steps every 30 s. **a** Current traces recorded on consecutive pulses (see numbers) applied to representative myocytes treated with 5 mM Cs^+ and 1 mM Ba^{2+}. *Dashed lines* indicate zero-current levels. **b** Time plot of current amplitude indicating an I_{ep} episode between 6 and 8 min in a myocyte treated with 5 mM Cs^+ at 0 min and Ba^{2+} at 11 min. **c** Types of I_{ep} episodes. Hyperpolarizing steps are represented by *filled circles*, and relative end-of-step I_{ep} amplitude is referenced to the *scale on the left*. *Numbers below the types* indicate their relative frequencies among 94 episodes from 81 experiments. Episodes in **a** (*left*) and **b** are examples of types 1 and 2, respectively

Number of Hyperpolarizations to Episode I_{ep}

We counted the hyperpolarizing steps that were applied up to and including the one that elicited the largest end-of-step I_{ep} amplitude in the first episode of an experiment. The number was dependent on bathing solution and voltage. For Na^+ solution, the numbers of steps were 8.2 ± 0.9 ($n = 10$) at −190 mV and 12.3 ± 1.4 ($n = 31$) at −160 mV; for $NMDG^+$ solution, the respective numbers were 8.6 ± 0.6 ($n = 24$) and 12.5 ± 1.5 ($n = 15$). The increase in steps at −160 mV was significant in both cases ($P < 0.02$, unpaired *t*-test with Welch correction). (An increase was also evident in the number of hyperpolarizations between the first and second episodes: 6.8 ± 0.8 [$n = 6$] at −190 mV, 10.3 ± 1.5 [$n = 7$] at −160 mV.) The number of steps to episode I_{ep} (−190 mV) in myocytes bathed with $NMDG^+ + La^{3+}$ solution was 12.8 ± 1.0 ($n = 20$), significantly longer ($P < 0.002$) than the number in myocytes bathed with $NMDG^+$ solution (8.6 ± 0.6 [$n = 24$]).

Incidence of I_{ep}

Percentage incidence data were compiled by scoring myocytes as I_{ep}-positive if they met the criterion $I_{ep} > 30$ pA at some point prior to voluntary or forced (apparent phase of deterioration) termination of an experiment. Observation times were approximately 15 min at −190/−160 mV (myocytes of Fig. 3c) and approximately 30 min at less negative potentials. When the incidence data for each solution were plotted against voltage, it was apparent that they could be fitted with a Boltzmann function: incidence = 100/(1 + exp((*V*$_{0.5}$ − *V*)/*S*)), where *V*$_{0.5}$ is the voltage at 50% incidence and *S* is the slope factor (Fig. 4). Na^+-solution data are well-described by a function with *V*$_{0.5}$ of −129.7 ± 1.4 mV and *S* of −7.9 ± 1.0 mV and $NMDG^+$ solution data, by a function with similar *S* (−7.2 ± 1.3 mV) but more negative *V*$_{0.5}$ (−146.3 ± 1.6 mV). The inclusion of 0.2 mM La^{3+} in $NMDG^+$ solution had little effect on *S* (−6.7 ± 1.0 mV) but a pronounced one on *V*$_{0.5}$ (−182.0 ± 1.4 mV).

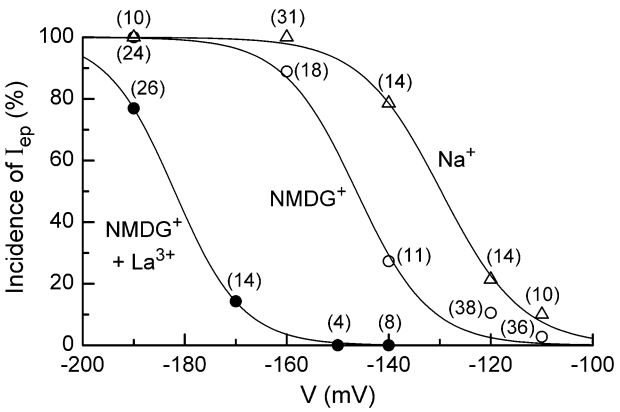

Fig. 4 Incidence of I_{ep}. Myocytes were bathed in Na^+, $NMDG^+$ or $NMDG^+ + La^{3+}$ (0.2 mM) solution and treated with 3–20 mM Cs^+ and 1–3 mM Ba^{2+}. Myocytes were held at −85 mV and hyperpolarized to a fixed voltage (*V*) for 200 ms every 30 s. Myocytes were scored as positive if $I_{ep} > 30$ pA was detected at some point during an experiment. The number of myocytes investigated is indicated in parentheses. The curves fitting data points are drawn in accord with incidence = 100/(1 + exp((*V*$_{0.5}$ − *V*)/S)), where *V*$_{0.5}$ is the voltage at 50% incidence and *S* is the slope factor. The *V*$_{0.5}$ values for the curves are (*left to right*) −182.0 ± 1.4, −146.3 ± 1.6 and −129.7 ± 1.4 mV and the corresponding *S* values are −6.7 ± 1.0, −7.2 ± 1.3 and −7.9 ± 1.0 mV

Amplitude of I_{ep}

Records from the same experiments used to determine I_{ep} incidence–voltage relations were used to evaluate the dependence of I_{ep} amplitude on voltage and external solution. The I_{ep} amplitude measured was the peak amplitude registered during any step over the course of an experiment, with the proviso that the current then decayed and was small or absent on four subsequent steps. The results (Fig. 5) point up the following: (1) at voltages ≥ -140 mV, peak I_{ep} was relatively small or absent; (2) at voltages < -140 mV, peak I_{ep} was smaller in myocytes bathed with $NMDG^+$ solution than in those bathed with Na^+ solution (e.g., -1.40 ± 0.22 nA [$n = 24$ $NMDG^+$] vs. -2.83 ± 0.34 nA [$n = 10$ Na^+] at -190 mV [$P < 0.01$, unpaired t-test with Welch correction]); and (3) peak I_{ep} at -190 mV was much smaller in myocytes bathed with $NMDG^+ + La^{3+}$ solution (-0.44 ± 0.10 nA [$n = 26$]) than in those bathed with $NMDG^+$ solution (-1.40 ± 0.22 nA [$n = 24$] [$P < 0.01$]).

Hyperpolarization-Induced I_{ep} in Myocytes Conditioned by Pulses to -100 mV

The foregoing findings on myocytes regularly pulsed to a fixed test potential such as -160 mV indicate that significant I_{ep} emerged after a series of conditioning pulses to that potential. To evaluate whether similar-sized I_{ep} emerges after conditioning to a less negative potential, groups of myocytes treated with Cs^+ and Ba^{2+} were conditioned with 200-ms pulses to -100 mV every 30 s and probed with one or more test pulses. The first group ($n = 7$) was bathed in $NMDG^+$ solution, conditioned for $\approx$7 min, probed with a 200-ms test pulse to -160 mV, conditioned for another 5 min and probed once more with a test pulse to -160 mV. The largest I_{ep} elicited by a test pulse was just -30 pA. The second group ($n = 12$) was bathed with Na^+ (or $NMDG^+$) solution for $\approx$7 min and then with $NMDG^+$ (or Na^+) solution for a further 7 min. The amplitudes of I_{ep} on single 300-ms test steps to -160 mV applied after each 7-min conditioning period were 159 ± 26 pA (Na^+) and 22 ± 6 pA ($NMDG^+$), i.e., far smaller than the respective amplitudes in myocytes conditioned at -160 mV (976 ± 180 [Na^+] and 452 ± 112 [$NMDG^+$]).

The third group ($n = 12$) was bathed in $NMDG^+ + La^{3+}$ solution, conditioned for 6–10 min and probed with 1,000-ms test pulses to -170, -190, -210 and -230 mV (30-s intervals). Peak I_{ep} amplitude on the test pulses to -190 mV (-29 ± 6 pA) was small compared to that observed in -190-mV conditioning experiments (-439 ± 105 pA). I_{ep} on the test pulse to -230 mV was -357 ± 119 pA, with most of the variability being due to a relatively large I_{ep} in two of the myocytes (e.g., Fig. 6a) and a very small I_{ep} in another. Records from the latter (Fig. 6b) are not unlike the records of single-channel currents from cell membrane patches, with possible millisecond-timescale unitary events (mean ≈ -8 pA [arrows, -190-mV trace]), multiples of these and bursting-like activity. Taking $i = -8$ pA (likely an underestimate due to recording bandwidth limitations) and $E_{rev} = -21.5$ mV gives a calculated "single-pore" conductance of $\approx$50 pS.

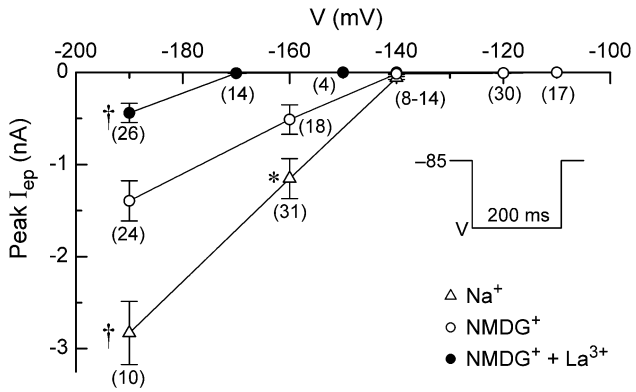

Fig. 5 Peak amplitude of I_{ep} in myocytes regularly pulsed with 200-ms hyperpolarizing steps (same myocytes and conditions as in Fig. 4). "Peak I_{ep}" refers to the maximum value of I_{ep} measured during an experiment, excluding any I_{ep} in an end-of-experiment deterioration phase. $^*P < 0.05$ (Na^+ vs. $NMDG^+$), $^\dagger P < 0.01$ (Na^+ vs. $NMDG^+$, $NMDG^+ + La^{3+}$ vs. $NMDG^+$) (unpaired t test with Welch correction)

Discussion

Hyperpolarization of guinea pig ventricular myocytes to voltages more negative than ≈ -140 mV elicited an irregular inward current that, on consideration of experimental conditions (presence of ion channel blockers, Na^+-free $NMDG^+$ solution) and other grounds (see "Results" section), was deemed much more likely to have been carried by hyperpolarization-induced electropores than by ion channels.

Electropores lined by the negatively charged head groups of membrane phospholipids are formed as a consequence of electric field-induced perturbation of membrane lipids (Vernier et al. 2004; Tarek 2005; Hu et al. 2006; Pakhomov et al. 2009; Wang et al. 2010). The threshold membrane potential for their formation is in the range of 250–1,000 mV, when cells are subjected to short-duration, high-strength external electrical fields (Wang et al. 2010). A similar threshold range for induction of high conductance in frog cardiac myocyte cell-attached patches subjected to approximately 5-ms voltage ramps and rectangular steps was reported by O'Neill and Tung (1991) and Tovar and Tung (1992). The lower "thresholds" for

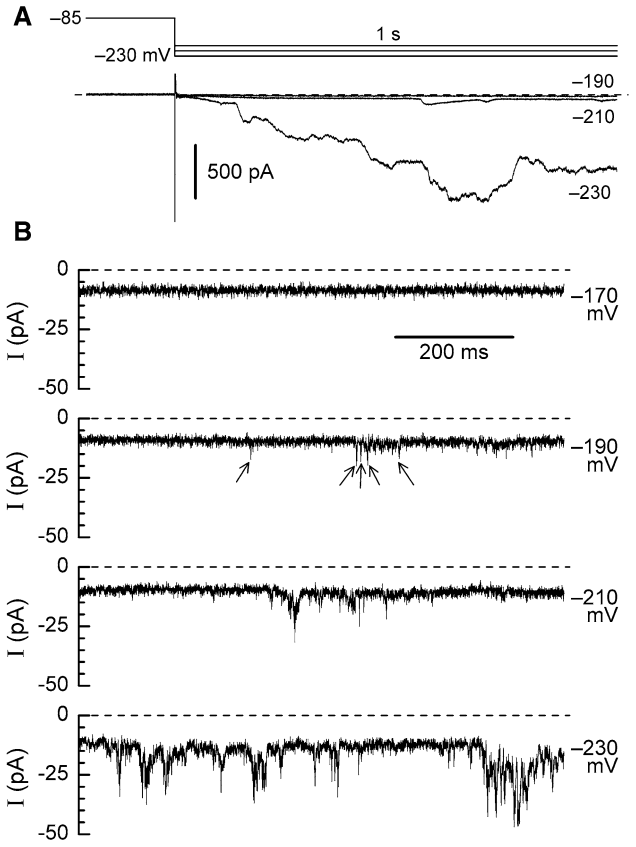

Fig. 6 I_{ep} elicited by 1-s test hyperpolarizations. Two myocytes were bathed with $NMDG^+ + La^{3+}$ solution, treated with 5 mM Cs^+ and 3 mM Ba^{2+} and pulsed from −85 to −100 mV for 200 ms every 30 s for ≈6 min prior to application of four 1,000-ms step hyperpolarizations to −170, −190, −210 and −230 mV at 30-s intervals. *Dashed lines* indicate zero-current levels. **a** Currents recorded from one of the myocytes. **b** Segments of test currents recorded from the other myocyte. *Arrows* point to unitary-like events (see text)

induction of significant I_{ep} in the guinea pig ventricular myocytes investigated here were most likely due to our use of much longer pulses than in the foregoing myocyte-patch studies. An example of the dependence of threshold on pulse duration comes from Troiano et al. (1998), who observed that the electroporation threshold of bilayer lipid membranes declined from 331 mV for 1-ms pulses to 167 mV for 10-s pulses.

Bonvallet and Christé (1988) presented clamp records from a frog atrial cell (17°C) in which three successive hyperpolarizations from −90 to −260 mV for 1.36 s at 30-s intervals elicited jagged inward currents, which they attributed to membrane breakdown. Ochi and colleagues (Akuzawa-Tateyama et al. 1998; Song and Ochi 2002) found that long-duration, relatively weak hyperpolarization triggered an electroporation current in whole cell–configured rabbit ventricular myocytes bathed in 0.1–0 mM K^+ solution at 23–25°C. In the first of their studies, the voltage was shifted by −10 mV every 30 s in staircase fashion, and the peak amplitude of irregular inward current elicited at each voltage was measured. For myocytes bathed in Na^+ solution, the amplitudes were "several nanoamperes" at −190 mV and approximately −1.7 nA at −170 mV, −0.2 nA at −160/−150 mV, −0.08 nA at −140 mV and −0.025 nA at −110 mV. In the present study, the peak amplitude of I_{ep} elicited by 200-ms hyperpolarizations applied every 30 s to myocytes bathed with Na^+ solution was about the same (−2.83 ± 0.34 nA) as the above at −190 mV, larger (−1.15 ± 0.22 nA) at −160 mV and about the same (−0.06 ± 0.02 nA) at −140 mV. A difference between the earlier results and those reported here concerns $NMDG^+$. Song and Ochi (2002) found that the amplitudes of I_{ep} in myocytes bathed with $NMDG^+$ solution were as large as those in myocytes bathed with Na^+ solution, whereas we found them to be considerably smaller. A possible factor in this divergence is that Song and Ochi (2002) did not compare Na^+ and $NMDG^+$ at potentials negative to −140 mV, which, in the present study, provided the evidence of smaller currents with $NMDG^+$ solution.

Our results are in good agreement with those of Akuzawa-Tateyama et al. (1998) in regard to the inhibitory action of La^{3+} on the amplitude of I_{ep}. They found that inclusion of 0.1 mM La^{3+} in Na^+ solution reduced peak amplitude from ≈−1,700 to −50 pA (−170 mV) and ≈−250 to −30 pA (−150 mV), whereas we found that inclusion of 0.2 mM La^{3+} in $NMDG^+$ solution reduced amplitude from ≈−800 pA (interpolated) to −14 ± 3 pA (−170 mV) and ≈−240 pA (interpolated) to <−10 pA (−150 mV). This "protective" effect of La^{3+} was observed against a background of possible protection afforded by millimolar Ca^{2+}, Mg^{2+}, Cd^{2+} and Ba^{2+} and was clearly reflected in a shift of the $V_{0.5}$ of the incidence of I_{ep} from −146.3 ± 1.6 mV to −182.0 ± 1.4 mV (Fig. 4). In considering how La^{3+} might inhibit I_{ep}, Akuzawa-Tateyama et al. (1998) cited a study indicating that La^{3+} accelerates fusion of acidic phospholipid membranes more effectively than Ca^{2+} by inducing a conformational change in the head region of the phospholipid that makes the membrane surface more hydrophobic (Ohki and Duax 1986) and suggested that this might accelerate the closure of electropores. More recently, La^{3+} has been shown to bind to the lipid bilayer and promote lateral compression and stabilization of the membrane (Cheng et al. 1999; Tanaka et al. 2001). A cocktail of 1 mM La^{3+} and 1 mM Gd^{3+} strongly inhibited nanosecond electrical pulse (nsEP)-induced decreases in the membrane resistance of GH3 cells (Pakhomov et al. 2007), and micromolar Gd^{3+} rapidly reversed nsEP-induced decreases in the membrane resistance of Jurkat cells (André et al. 2010). The latter findings suggest that lanthanides can both inhibit the formation of electropores and shorten their lifetimes.

When myocytes superfused with Na^+ or $NMDG^+$ solution were pulsed from a holding potential of −85 mV to a fixed voltage <−140 mV with 200-ms steps every 30 s, the I_{ep} elicited by the steps was very small or absent for a number of steps and then relatively large during the next one to three steps (Fig. 3). The average number of hyperpolarizing steps to a large I_{ep} was dependent on voltage (e.g., 8.6 ± 0.6 and 12.5 ± 1.5 at −190 and −160 mV, respectively) but not on the principal cation. It may be that each hyperpolarization promotes disarrangement of membrane lipid, that there is a certain probability that this leads to formation of hydrophilic pores (see Chernomordik et al. 1987; Escoffre et al. 2007) and that this probability increases with negative voltage.

In the majority of occurrences (episodes) of I_{ep} in myocytes pulsed to −160 mV, a large I_{ep} on one step was followed by a small or no I_{ep} on the next one (Fig. 3c). This observation suggests that electropore number/size shrank during the interstep interval at −85 mV and did not expand again on the next step (as though large I_{ep} relieved hyperpolarization-induced membrane stress (see Escoffre et al. 2007)). In other episodes, this refractory state was only attained after several interstep intervals/I_{ep}-inducing steps.

Inclusion of La^{3+} in $NMDG^+$ solution had significant effects on the timing and pattern of episodes. It increased the number of steps to the first episode at −190 mV from 8.6 ± 0.6 ($n = 24$) to 12.8 ± 1.0 ($n = 20$), suggesting inhibition of lipid disarrangement and/or subsequent pore formation. In addition, it increased the percentage of off–on–off and off–on–on–off episodes (−190 mV) from 33 and 4% (control $NMDG^+$) to 64 and 20%, respectively. These results support the suggestion by Akuzawa-Tateyama et al. (1998) that La^{3+} promotes closure of electropores.

Song and Ochi (2002) found that (ramp-evaluated) E_{rev} of I_{ep} in myocytes dialyzed with an approximately 130-mM KCl solution and bathed with NaCl solution was −0.7 ± 3.5 mV and that 90% replacement of pipette Cl^- by aspartate (Asp^-) had little effect on E_{rev}. In the present study, E_{rev} in myocytes dialyzed with a 140-mM K^+, 30-mM Cl^-, 110-mM Asp^- solution and bathed with NMDG-Cl solution was −21.5 ± 1.5 mV. These two E_{rev} values can be considered under two scenarios: (1) electropores are not lined with the negatively charged heads of phospholipids and (2) electropores are charge-lined.

1. *Non-charge-lined electropores.* If electropores are not lined with negative charges, relatively large $NMDG^+$ and Asp^- should be less permeable than small K^+ and Cl^-. Calculations with the GHK equation (Hille 2001) and $E_{rev} = -21.5$ mV led to the conclusion that the larger P_{Asp}/P_{Cl}, the smaller P_{NMDG}/P_K for any given P_{Cl}/P_K up to 1.0; for $P_{Cl}/P_K \approx 1$ and a reasonable P_{Asp}/P_{Cl} of 0.2–0.4, P_{NMDG}/P_K is 0.5–0.34.
2. *Charge-lined electropores*. Since pores lined with negatively charged moieties greatly restrict passage of anions, calculations with the GHK equation and the foregoing E_{rev} values point to $P_{Na} \approx P_K$ (earlier study) and $P_{NMDG} \approx 0.4P_K$ (this study). Consequently, the Song and Ochi (2002) interpretation of the lack of effect of Asp^- replacement of Cl^- on E_{rev}, i.e., that $P_{Asp} \approx P_{Cl}$ ($\approx P_{Na}$), can instead be taken as evidence that neither of these anions was very permeable. The fact that electropores have wider pores than most cation-selective channels does not mean that they necessarily have weak cation selectivity. This contention is supported by the following examples: (1) agonist-induced dilation of the pore of the cation-selective P2X7 receptor channel increases permeability to $NMDG^+$ (e.g., from 0.03 to 0.3 P_{Na} in 30 s; MacKenzie et al. 1998) without simultaneously increasing permeability to Cl^- (Li et al. 2005), (2) agonist-induced dilation of the TRPA1 channel pore increased P_{NMDG}/P_{Na} from 0.05 ± 0.003 to 0.22 ± 0.013 without affecting low P_{Cl} (Chen et al. 2009) and (3) despite their having nanometer-diameter pores (passage of ions and neutral solutes up to ≈650 Da), bacterial OmpF channels exhibit strong cation selectivity ($P_{Cl}/P_K < 0.1$ [≈0.1-M solutions]) (Danelon et al. 2003; Alcaraz et al. 2004). A more rigorous analysis of cation and anion permeation through electropores is provided in Appendix.

In summary, both this study and the earlier ones (Akuzawa-Tateyama et al. 1998; Song and Ochi 2002) on guinea pig ventricular myocytes indicate that hyperpolarization can trigger I_{ep}, whose size is dependent on the voltage protocol. The I_{ep} can distort records of ionic currents frequently investigated at strongly hyperpolarized potentials (e.g., I_{K1}, Fig. 1, and I_f, see Ranjan et al. 1998) and likely those closer to resting potential in myocytes affected by intracellular or extracellular bilayer-active agents (e.g., Song and Ochi 2002).

Acknowledgments We thank Svetlana Zhabeeva for excellent technical assistance. This work was supported by the Heart and Stroke Foundation of New Brunswick and the Canadian Institutes of Health Research.

Appendix

Simulation of Dependence of Reversal Potential of Multi-Ionic Current on Pore Diameter

The reversal potential (E_{rev}) of a multi-ionic current is determined by the composition of the solutions on the two sides of the membrane and the relative permeabilities of

the charge-carrying ions. Applying standard GHK assumptions of independence and constant field (Hille 2001), E_{rev} can be calculated from solution composition[1] and the relative permeabilities of ions:

$$E_{rev} = -61 \log \frac{K_i^+ + (P_{Cl}/P_K) \cdot Cl_o^-}{(P_{NMDG}/P_K) \cdot NMDG_o^+ + (P_{Cl}/P_K) \cdot Cl_i^- + (P_{ASP}/P_K) \cdot Asp_i^-} \quad (1)$$

Assuming that relative permeabilities are determined by steric and/or electrostatic interactions of ions and the pore, they can be estimated from the effective diameters of charge carriers, diameter of the pore and charges lining the pore by employing excluded-area theory (Sabovcik et al. 1995) with the modification that "effective" rather than crystal diameters of ions are used to take account of ion–pore interaction. Thus, the relative permeability (P_X/P_Y) of ions X (effective diameter δ_X) and Y (effective diameter δ_Y) through a pore of diameter d_{pore} is given by

$$\frac{P_X}{P_Y} = \frac{(d_{pore} - \delta_X)^2}{(d_{pore} - \delta_Y)^2} \quad (2)$$

The effective diameter of an ion depends on the nature of the ion–pore interaction, which determines whether the ion passes in hydrated form or not. If the ion has a hydrated shell, its effective diameter is given by the Debye length (δ) of the solution times 2. This can be envisioned as an ion with crystal radius r carrying a layer of water (thickness $\delta - r$) sufficient to isolate it from other charges in the solution and/or within the pore. If an ion already has a radius larger than the Debye length, it is considered to be sufficiently isolated and to have an effective diameter equal to the crystal diameter. The Debye length (δ) is a function of ionic strength ($I = 0.152$ M), absolute temperature ($T = 273.15 + 35.5$ K) and relative permittivity ($\varepsilon_r = 80$ for bulk water and 4–20 for water in small pockets within or around proteins) as follows:

$$\delta = \left(\frac{\varepsilon_0 \varepsilon_r kT}{2N_A q_e I}\right)^{1/2} \quad (3)$$

where ε_0, k, N_A, and q_e are permittivity of vacuum, Boltzmann constant, Avogadro number and elementary charge, respectively.

We consider two cases below, non-charge-lined electropores and charge-lined electropores, and use the foregoing framework to generate plots of the dependence of E_{rev} on pore size for selected values of ε_r and to determine possible pore size from intercepts with experimentally determined $E_{rev} = -21.5$ mV.

Non-Charge-Lined Electropores

Assuming that hydrophobic pores cannot strip ions of their hydration shells (i.e., cations and anions pass through the pore fully hydrated), an estimate of 2δ with ε_r for bulk water gives $2\delta = 16$ Å; i.e., all of the ions involved have the same effective diameter and $E_{rev} = 0$ for all pores >16 Å (clearly not the case for this study). Moreover, under this framework all involved ions have the same diameter until ε_r is sufficiently small to give $2\delta < d_{NMDG}$ ($NMDG^+$ is the ion with the largest crystal diameter); for $d_{NMDG} = 6.8$ Å, this occurs when $\varepsilon_r < 14.4$. On the other hand, the difference in diameters between ions has to be sufficiently large to generate $E_{rev} = -21.5$ mV. For example, $\varepsilon_r \approx 9$ is the largest ε_r that will give the $2\delta = 5.38$ Å (smaller than d_{NMDG} and d_{Asp} but larger than d_K and d_{Cl}) required for $E_{rev} =$ –21.5 mV with pore diameter 7.1 Å. For $\varepsilon_r = 4$, 2δ is 3.59 Å (smaller than d_{NMDG}, d_{Asp} and d_{Cl} but larger than d_K) and pore diameter 10.33 Å gives $E_{rev} = -21.5$ mV (see Table 1 for δ_{ion}) (d_{ion} or 2δ whichever is greater), 2δ and E_{rev} values for ε_r 80, 14.4, 9 and 4; E_{rev} as a function of d_{pore} for $\varepsilon_r = 9$ and $\varepsilon_r = 4$ is plotted in Fig. 7a.

Charge-Lined Pore

We assume that charge-lined electropores pass dehydrated cations (charges within the pore provide sufficient energy for cations to shed their hydration shells) and, perhaps, fully hydrated anions. Consequently, we use the crystal diameter for cations and δ_{ion} for anions. For $\varepsilon_r = 80$ (bulk water), δ_{Cl} and δ_{Asp} are 16 Å; i.e., pores with diameter

Table 1 Non-charge-lined pore: values of 2δ, δ_{ion} and E_{rev} (d_{pore}) for selected values of ε_r

ε_r	2δ (Å)	δ_K (Å)	δ_{Cl} (Å)	δ_{NMDG} (Å)	δ_{Asp} (Å)	E_{rev}, mV (d_{pore}, Å)
80	16	16	16	16	16	0 (>16)
14.4	6.8	6.8	6.8	6.8	6.8	0 (>6.8)
9	5.378	5.378	5.378	6.8	5.54	–21.5 (7.1)
4	3.585	3.585	3.64	6.8	5.54	–21.5 (10.33)

[1] Dialysate: 140 mM K^+, 30 mM Cl^-, 110 mM aspartate (Asp^-). Superfusate: 140 mM NMDG-Cl. Divalent species are present in relatively low concentrations and are not considered.

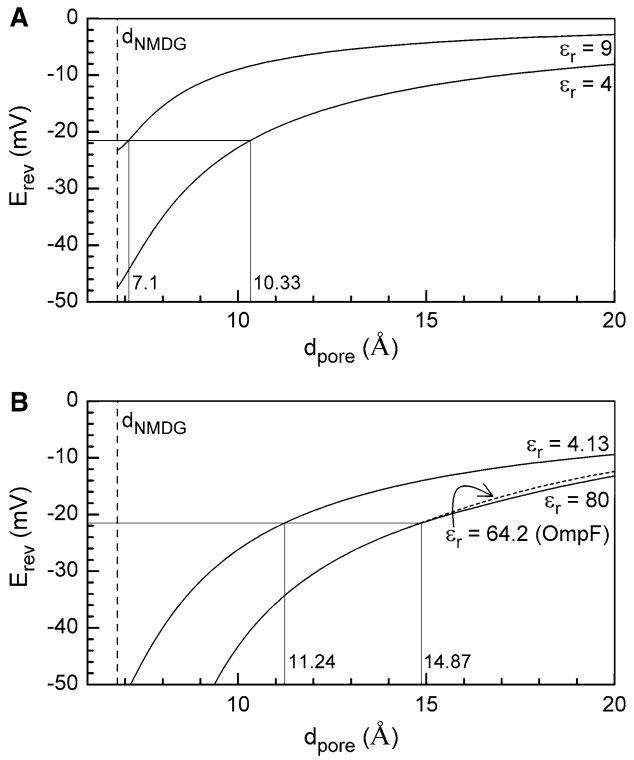

Fig. 7 Simulations of the dependence of E_{rev} on pore diameter (d_{pore}). *Vertical dashed lines* indicate minimal pore diameter equal to d_{NMDG}. *Straight lines within plots* extend to $E_{rev} = -21.5$ mV and corresponding pore diameters. **a** Dependence of E_{rev} on d_{pore} for non-charge-lined pore in which $\varepsilon_r = 4$ and $\varepsilon_r = 9$. **b** Dependence of E_{rev} on d_{pore} for charge-lined pore in which (1) $\varepsilon_r = 4.13$ and $\varepsilon_r = 80$ (*solid curves*) and (2) $\varepsilon_r = 64.2$ (estimated for OmpF pore) (*dashed curve*)

<16 Å pass cations only. For this ε_r, $E_{rev} = -21.5$ mV is achieved for a pore of 14.87 Å. However, since we do not know whether charge-lined electropores have an ε_r as high as that of bulk solution, we need to examine the influence of lower ε_r on pore diameter. It turns out that lowering ε_r decreases the effective size of anions and increases anion permeability. These increases are associated with three "threshold" values of ε_r. At the first threshold ($\varepsilon_r = 68.82$), the effective diameter of anions (2δ) becomes equal to 14.87 Å, i.e., the diameter of the cationic pore that has $E_{rev} = -21.5$ mV. This means that, for $\varepsilon_r < 68.82$ to achieve $E_{rev} = -21.5$ mV, the pore needs to pass anions; thus, anion permeability ($P_{Cl} = P_{Asp}$ since $\delta_{Cl} = \delta_{Asp}$) increases from 0 until ε_r reaches the second threshold. At the second threshold ($\varepsilon_r = 9.55$), the effective diameter of anions is equal to the crystal diameter of Asp^- ($2\delta = \delta_{Asp} = 5.54$ Å). This results in maximal P_{Asp}, whereas for $\varepsilon_r < 9.55$ P_{Cl} increases and $P_{Cl} > P_{Asp}$ until ε_r reaches the third threshold. At the third threshold ($\varepsilon_r = 4.13$), $2\delta = \delta_{Cl} = 3.64$ Å and P_{Cl} is maximal; further lowering of ε_r has no effect on estimated d_{pore} ($d_{pore} = 11.22$ Å for $E_{rev} = -21.5$ mV). Values of δ_{ion} (d_{ion} or 2δ, whichever is greater), 2δ and E_{rev} for the selected ε_r are summarized in Table 2; and E_{rev} as a function of d_{pore} for ε_r 80 and 4.13 is plotted in Fig. 7b.

Estimation of ε_r for Charge-Lined Pore

The present framework can be used to estimate ε_r for a charge-lined pore of known size and known P_{cation}/P_{anion} value. At its narrowest region, the bacterial porin OmpF is 7 × 11 Å (Cowan et al. 1992) (effective $d_{pore} = (7 \times 11)^{1/2} = 8.77$ Å) and has negative charges (−2) (Alcaraz et al. 2004). Estimated $P_{Na}/P_{Cl} = 4.5$ (1 M NaCl solution) (Saint et al. 1996; Phale et al. 2001; Danelon et al. 2003) requires that δ_{Cl} be 5.6 Å, values that correspond to $\varepsilon_r = 64.2$. Using this ε_r as an estimate of ε_r within an electropore results in (1) 2δ (0.152 M) of 14.36 Å (i.e., $\delta_{Cl} = \delta_{Asp} = 2\delta$), (2) pore diameter 14.85 Å for $E_{rev} = -21.5$ mV, (3) $P_{Cl}/P_K = P_{Asp}/P_K \approx 0.0016$ and (4) $P_{NMDG}/P_K = 0.44$.

Summary

Non-charge-lined electropores can achieve the selectivity required to attain $E_{rev} = -21.5$ mV but only with extremely low values of ε_r and a pore diameter close to that of the crystal diameter of $NMDG^+$. On the other hand, charge-lined electropores can achieve the desired selectivity at ε_r as high as that of bulk solution. Application of $\varepsilon_r = 64.2$ (estimated for bacterial porin OmpF) to the

Table 2 Charge-lined pore: values of 2δ, δ_{ion} and d_{pore} for $E_{rev} = -21.5$ mV and selected ε_r

ε_r	2δ (Å)	δ_K (Å)	δ_{Cl} (Å)	δ_{NMDG} (Å)	δ_{Asp} (Å)	d_{pore} ($E_{rev} = -21.5$ mV) (Å)
80	16	2.76	16	6.8	16	14.87
68.82	14.87	2.76	14.87	6.8	14.87	14.87
9.55	5.54	2.76	5.54	6.8	5.54	10.37
4.13	3.64	2.76	3.64	6.8	5.54	11.24

charge-lined electropore suggests that it has a diameter of 14.85 Å, is strongly cation-selective ($P_{Cl}/P_K = P_{Asp}/P_K \approx 0.0016$) and has $P_{NMDG}/P_K = 0.44$.

References

Abidor I, Arakelyan V, Chernomordik L et al (1979) Electrical breakdown of bilayer lipid membranes: I. The main experimental facts and their qualitative discussion. J Electroanal Chem 104:37–52

Akuzawa-Tateyama M, Tateyama M, Ochi R (1998) Low K^+-induced hyperpolarizations trigger transient depolarizations and action potentials in rabbit ventricular myocytes. J Physiol 513:775–786

Alcaraz A, Nestorovich EM, Aguilella-Arzo M et al (2004) Salting out the ionic selectivity of a wide channel: the asymmetry of OmpF. Biophys J 87:943–957

Al-Khadra A, Nikolski V, Efimov IR (2000) The role of electroporation in defibrillation. Circ Res 87:797–804

André FM, Rassokhin MA, Bowman AM et al (2010) Gadolinium blocks membrane permeabilization induced by nanosecond electric pulses and reduces cell death. Bioelectrochemistry 79:95–100

Bonvallet R, Christé G (1988) Membrane responses to large hyperpolarizations in trabecles and single cells of frog atrium. Gen Physiol Biophys 7:433–447

Chen C, Smye SW, Robinson MP et al (2006) Membrane electroporation theories: a review. Med Biol Eng Comput 44:5–14

Chen J, Kim D, Bianchi BR et al (2009) Pore dilation occurs in TRPA1 but not in TRPM8 channels. Mol Pain 5:3

Cheng Y, Yao H, Lin H et al (1999) The events relating to lanthanide ions enhanced permeability of human erythrocyte membrane: binding, conformational change, phase transition, perforation and ion transport. Chem Biol Interact 121:267–289

Chernomordik LV, Sukharev SI, Popov SV et al (1987) The electrical breakdown of cell and lipid membranes: the similarity of phenomenologies. Biochim Biophys Acta 902:360–373

Clapp LH (1995) Regulation of glibenclamide-sensitive K^+ current by nucleotide phosphates in isolated rabbit pulmonary myocytes. Cardiovasc Res 30:460–468

Cowan SW, Schirmer T, Rummel G et al (1992) Crystal structures explain functional properties of two *E. coli* porins. Nature 358:727–733

Danelon C, Suenaga A, Winterhalter M et al (2003) Molecular origin of the cation selectivity in OmpF porin: single channel conductances vs. free energy calculation. Biophys Chem 104:591–603

Del Castillo J, Katz B (1954) Changes in end-plate activity produced by presynaptic polarization. J Physiol 124:586–604

Dev S, Rabussay D, Widera G et al (2000) Medical applications of electroporation. IEEE Trans Plasma Sci 28:206–223

Escoffre JM, Dean DS, Hubert M et al (2007) Membrane perturbation by an external electric field: a mechanism to permit molecular uptake. Eur Biophys J 36:973–983

Fedorov VV, Nikolski VP, Efimov IR (2008) Effect of electroporation on cardiac electrophysiology. Methods Mol Biol 423:433–448

Gwanyanya A, Amuzescu B, Zakharov SI et al (2004) Magnesium-inhibited, TRPM6/7-like channel in cardiac myocytes: permeation of divalent cations and pH-mediated regulation. J Physiol 559:761–776

Hagiwara N, Irisawa H (1989) Modulation by intracellular Ca^{2+} of the hyperpolarization-activated inward current in rabbit single sino-atrial node cells. J Physiol 409:121–141

Harrison RL, Byrne BJ, Tung L (1998) Electroporation-mediated gene transfer in cardiac tissue. FEBS Lett 435:1–5

Harvey RD, Ten Eick RE (1989) Voltage-dependent block of cardiac inward-rectifying potassium current by monovalent cations. J Gen Physiol 94:349–361

Heller LC, Heller R (2006) In vivo electroporation for gene therapy. Hum Gene Ther 17:890–897

Hille B (2001) Ion channels of excitable membranes, 3rd edn. Sinauer Associates, Sunderland, MA

Hodgkin AL (1947) The membrane resistance of a non-medullated nerve fibre. J Physiol 106:305–318

Hu Q, Sridhara V, Joshi R et al (2006) Molecular dynamics analysis of high electric pulse effects on bilayer membranes containing DPPC and DPPS. IEEE Trans Plasma Sci 34:1405–1411

Huang C, Wheeldon L, Thompson TE (1964) The properties of lipid bilayer membranes separating two aqueous phases: formation of a membrane of simple composition. J Mol Biol 8:148–160

Huang ZM, Prasad C, Britton FC et al (2009) Functional role of CLC-2 chloride inward rectifier channels in cardiac sinoatrial nodal pacemaker cells. J Mol Cell Cardiol 47:121–132

Isenberg G (1993) Nonselective cation channels in cardiac and smooth muscle cells. EXS 66:247–260

Jones JL, Lepeschkin E, Jones RE et al (1978) Response of cultured myocardial cells to countershock-type electric field stimulation. Am J Physiol Heart Circ Physiol 235:H214–H222

Jones JL, Jones RE, Balasky G (1987) Microlesion formation in myocardial cells by high-intensity electric field stimulation. Am J Physiol Heart Circ Physiol 253:H480–H486

Kim JM, Lim BK, Ho SH et al (2006) TNFR-Fc fusion protein expressed by in vivo electroporation improves survival rates and myocardial injury in coxsackievirus induced murine myocarditis. Biochem Biophys Res Commun 344:765–771

Kinosita K, Tsong TY (1977) Formation and resealing of pores of controlled sizes in human erythrocyte membrane. Nature 268:438–441

Kitamura K, Judkewitz B, Kano M et al (2008) Targeted patch-clamp recordings and single-cell electroporation of unlabeled neurons in vivo. Nat Methods 5:61–67

Kiyosue T, Spindler AJ, Noble SJ et al (1993) Background inward current in ventricular and atrial cells of the guinea pig. Proc Biol Sci 252:65–74

Li Q, Luo X, Muallem S (2005) Regulation of the P2X7 receptor permeability to large molecules by extracellular Cl^- and Na^+. J Biol Chem 280:26922–26927

MacKenzie A, Virginio C, North R, et al (1998) The rat P2X7 receptor: characterization of pore formation. J Physiol 506P:45P

Noma A, Shibasaki T (1985) Membrane current through adenosine-triphosphate-regulated potassium channels in guinea pig ventricular cells. J Physiol 363:463–480

O'Neill RJ, Tung L (1991) Cell-attached patch clamp study of the electropermeabilization of amphibian cardiac cells. Biophys J 59:1028–1039

Ohki S, Duax J (1986) Effects of cations and polyamines on the aggregation and fusion of phosphatidylserine membranes. Biochim Biophys Acta 861:177–186

Ooyama H, Wright EB (1961) Anode break excitation on single Ranvier node of frog nerve. Am J Physiol 200:209–218

Pakhomov AG, Shevin R, White JA et al (2007) Membrane permeabilization and cell damage by ultrashort electric field shocks. Arch Biochem Biophys 465:109–118

Pakhomov AG, Bowman AM, Ibey BL et al (2009) Lipid nanopores can form a stable, ion channel-like conduction pathway in cell membrane. Biochem Biophys Res Commun 385:181–186

Phale PS, Philippsen A, Widmer C et al (2001) Role of charged residues at the OmpF porin channel constriction probed by mutagenesis and simulation. Biochemistry 40:6319–6325

Ranjan R, Chiamvimonvat N, Thakor NV et al (1998) Mechanism of anode break stimulation in the heart. Biophys J 74:1850–1863

Sabovcik R, Li J, Kucera P et al (1995) Permeation properties of a Ca^{2+}-blockable monovalent cation channel in the ectoderm of the chick embryo: pore size and multioccupancy probed with organic cations and Ca^{2+}. J Gen Physiol 106:149–174

Saint N, Lou KL, Widmer C et al (1996) Structural and functional characterization of OmpF porin mutants selected for larger pore size. II. Functional characterization. J Biol Chem 271:20676–20680

Sale AJH, Hamilton WA (1967) Effects of high electric fields on microorganisms. I. Killing bacteria and yeasts. Biochim Biophys Acta 148:781

Schoenbach KH, Joshi R, Stark RH (2000) Bacterial decontamination of liquids with pulsed electric fields. IEEE Trans Dielectr Electr Insul 7:637–645

Schoenbach KH, Joshi R, Kolb J et al (2004) Ultrashort electrical pulses open a new gateway into biological cells. Proc IEEE 92:1122–1137

Sersa G, Miklavcic D, Cemazar M et al (2008) Electrochemotherapy in treatment of tumours. Eur J Surg Oncol 34:232–240

Song YM, Ochi R (2002) Hyperpolarization and lysophosphatidylcholine induce inward currents and ethidium fluorescence in rabbit ventricular myocytes. J Physiol 545:463–473

Stämpfli R (1958) Reversible electrical breakdown of the excitable membrane of a Ranvier node. An Acad Bras Cienc 30:57–63

Tanaka T, Li SJ, Kinoshita K et al (2001) La^{3+} stabilizes the hexagonal II (H(II)) phase in phosphatidylethanolamine membranes. Biochim Biophys Acta 1515:189–201

Tarek M (2005) Membrane electroporation: a molecular dynamics simulation. Biophys J 88:4045–4053

Tien HT, Diana AL (1967) Black lipid membranes in aqueous media: the effect of salts on electrical properties. J Colloid Interface Sci 24:287–296

Tovar O, Tung L (1992) Electroporation and recovery of cardiac cell membrane with rectangular voltage pulses. Am J Physiol Heart Circ Physiol 263:H1128–H1136

Troiano GC, Tung L, Sharma V et al (1998) The reduction in electroporation voltages by the addition of a surfactant to planar lipid bilayers. Biophys J 75:880–888

Tsong TY (1983) Voltage modulation of membrane permeability and energy utilization in cells. Biosci Rep 3:487–505

Tung L (1992) Electrical injury to heart muscle cells. In: Lee RC, Cravalho EG, Burke JF (eds) Electrical trauma the pathophysiologymanifestations and clinical management. Cambridge University Press, Cambridge, pp 361–400

Uesaka N, Nishiwaki M, Yamamoto N (2008) Single cell electroporation method for axon tracing in cultured slices. Dev Growth Differ 50:475–477

Vernier PT, Sun Y, Marcu L et al (2004) Nanosecond pulsed electric fields perturb membrane phospholipids in T lymphoblasts. FEBS Lett 572:103–108

Wang M, Orwar O, Olofsson J et al (2010) Single-cell electroporation. Anal Bioanal Chem 397:3235–3248

Yu H, Chang F, Cohen IS (1993) Pacemaker current exists in ventricular myocytes. Circ Res 72:232–236

Zimmermann U, Riemann F, Pilwat G (1976) Enzyme loading of electrically homogeneous human red blood cell ghosts prepared by dielectric breakdown. Biochim Biophys Acta 436:460–474